

nNxB: a new coarse-grained model for RNA and DNA nanotechnology

F. Tosti Guerra,¹ E. Poppleton,^{2,3} P. Šulc,^{2,4} and L. Rovigatti¹

¹⁾*Department of Physics, Sapienza University of Rome*

²⁾*School of Molecular Sciences and Center for Molecular Design and Biomimetics, The Biodesign Institute, Arizona State University*

³⁾*Biophysical Engineering Group, Max Planck Institute for Medical Research*

⁴⁾*Department of Bioscience, School of Natural Sciences, Technical University Munich*

(Dated: November 7, 2023)

The folding processes of RNA and DNA play crucial roles in biological systems and nanotechnology. However, studying these processes with high-resolution models is beyond current computational capabilities. In this article, we present a new coarse-grained model for investigating the folding dynamics of nucleic acids. Our model represents n nucleotides using a single patchy particle and is parametrized using well-established nearest-neighbor models. By simplifying the system and interactions, our model allows for simulations at timescales and length scales that are currently inaccessible to more detailed models. To validate the performance of our model, we conducted extensive simulations of various single-stranded systems. We examined the thermodynamics of DNA hairpins, capturing their stability and structural transitions. We also investigated the folding of an MMTV pseudoknot, a complex RNA structure involved in viral replication. Furthermore, we explored the folding of a challenging RNA tile containing a k-type pseudoknot. The new coarse-grained model accurately captures the folding behavior of diverse nucleic acid structures, providing insights into their thermodynamics. The successful reproduction of experimental data and favorable comparisons with existing coarse-grained models validate the effectiveness of our approach.

I. INTRODUCTION

RNA and DNA molecules play critical roles in biological systems and have become increasingly important in constructing nanoscale architectures^{1,2}. Understanding the folding processes of these molecules is essential for unraveling their functional mechanisms and facilitating the design of innovative nanoscale structures, with broad implications across scientific disciplines. One significant application of understanding folding pathways is in RNA and DNA structure prediction, since kinetic traps can prevent access to the conformation corresponding to absolute free-energy minima. Accurately predicting secondary and tertiary structures is crucial for elucidating their biological functions, designing therapeutic interventions, engineering RNA/DNA-based nanomaterials³, facilitating vaccine delivery⁴, and improving drug delivery⁵.

Another area where knowledge of folding pathways is valuable is functional RNA design. RNA molecules have diverse functional roles, including catalysis, gene regulation, and molecular recognition⁶. Understanding folding pathways enables the rational design of functional RNA structures with desired properties, such as enhanced catalytic activity or improved binding affinity to specific targets⁷.

Finally, the use of RNA and DNA in nanotechnology is gaining traction, as they serve as versatile building blocks for constructing a wide range of nanoscale devices and materials⁸. These include self-assembling complex 2D and 3D architectures using DNA origami^{2,9,10}, dynamic structures like DNA motors^{11–13}, and even DNA-based computational systems^{14–16}. Exploring the intricate folding pathways of RNA and DNA helps uncover fundamental principles of self-assembly, enabling the design of increasingly complex and programmable nanostructures with exciting possibilities for applications in various fields.

Computational models have been developed to explore the processes involved in RNA and DNA folding. These models range from atomistic to coarse-grained resolutions, each offering unique advantages and insights into the dynamics of folding. The all-atom model is a commonly employed approach that explicitly represents individual atoms and their interactions. Atomistic force fields such as AMBER¹⁷ and CHARMM¹⁸ have been extensively used to investigate the folding of nucleic acids¹⁹. While these models accurately capture atomistic details and provide valuable insights into the structural and energetic aspects of RNA and DNA, their simulations are computationally demanding and limited in timescale.

To overcome the limitations of all-atom models, coarse-grained models have emerged as powerful tools for studying longer lengths and timescales of nucleic acid folding. Coarse-grained models simplify the representation of nucleic acids by grouping multiple atoms into a single particle or bead, allowing for more efficient simulations and exploration of extended timescales. Several coarse-grained models have been specifically developed for studying DNA and RNA^{20–41}.

Coarse-grained models offer a reduced number of degrees of freedom compared to atomistic approaches when representing DNA/RNA. They typically treat the solvent and solvated ions implicitly and represent groups of atoms in the DNA/RNA structure with effective interactions. This simplification enables the study of larger and more extended molecular systems for longer times. Coarse-graining techniques can be broadly categorized as either from a bottom-up or top-down, each aiming to capture specific aspects of the system. The bottom-up approach formally maps the statistical behavior of a more detailed model into a coarse-grained description, while the top-down approach aims to reproduce as many experimentally relevant properties as possible⁴².

Many of the models mentioned above are parametrized using nearest-neighbor (NN) models. Initially introduced by Poland and Scheraga to investigate duplex denaturation phase transitions⁴³, this approach has been meticulously parameterized^{44–53} to describe binding equilibria for oligonucleotides.

A nearest-neighbor model calculates the free energy change (ΔG) associated with forming a duplex by summing the contributions of individual base pair interactions. These interactions are characterized by experimentally determined enthalpy (ΔH_{ij}) and entropy (ΔS_{ij}) values for each possible combination of adjacent base pairs (i, j) . Different base pair combinations have different thermodynamic parameters, reflecting variations in hydrogen bonding, stacking interactions, and other factors.

The concentration of the fully bound duplex product, denoted as $[AB]$, is related to the thermodynamic parameters and the equilibrium constant (K) of the duplex formation. The equilibrium constant is defined as the ratio of the concentration of the product $[AB]$ to the concentrations of the individual strands $[A]$ and $[B]$:

$$K = \frac{[AB]}{[A][B]} \propto \exp(-\beta(\Delta H - T\Delta S)), \quad (1)$$

where ΔH and ΔS are the total enthalpy and entropy change upon binding, and $\beta = 1/k_B T$.

By considering nearest-neighbor interactions along the entire sequence length, the model predicts the stability of duplexes and provides insights into their melting temperatures, binding affinities, and overall thermodynamic properties.

In our study, we introduce a new coarse-grained description of nucleic acids where a single patchy particle represents n nucleotides, enabling efficient exploration of RNA and DNA folding processes. We parametrize our model using well-established nearest-neighbor models^{44–49,53} to capture essential interactions involved in folding dynamics while maintaining computational efficiency. Our model combines the strengths of existing coarse-grained and patchy particle models, providing new possibilities for investigating folding phenomena at previously inaccessible time- and length-scales. This first iteration of the model has been parametrized by considering single-stranded systems only, and its thermodynamic performance has been compared with available experimental and numerical data.

II. MODEL DESCRIPTION

In our model, we introduce a polymer composed of N beads to represent the DNA/RNA strand. Each bead is decorated with an attractive spherical patch, having a radius of 0.219σ and positioned $\delta_{pb} = 0.65\sigma$ away from the center of the bead, and represents n nitrogenous bases that make up the nucleic acid molecule. We incorporate several potentials to reproduce the thermodynamic and mechanical characteristics of these biopolymers.

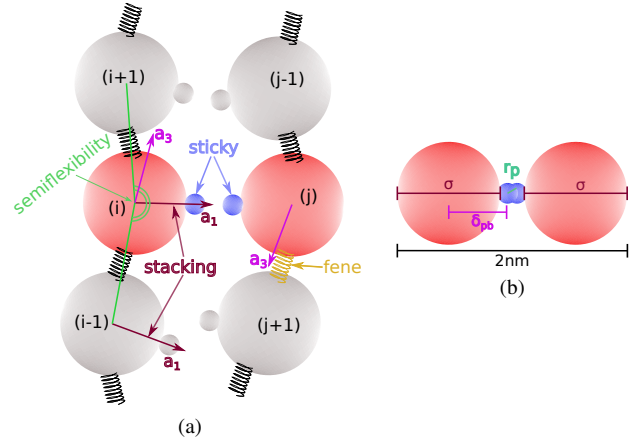


Figure 1. (a) schematic representation of the attractive interaction in nNxB, (b) the diameter of the DNA/RNA helix is approximately 2 nm. Considering our beads with a diameter denoted as σ and the patches on the beads' surface with a diameter of $r_p = 0.219\sigma$, we can determine that $2\sigma + 2\sigma(\delta_{pb} - 0.5) + r_p\sigma = 2$ nm. Therefore, we can deduce that $\sigma = 2/(1 + 2\delta_{pb} + r_p)$ nm.

Figure 1 provides a visual summary of the notation and different interaction terms used in our model, while the detailed functional forms are reported in Appendix A. The potentials between topologically bonded beads linked through the backbone include the Kremer-Grest force field⁵⁴, combining a Weeks-Chandler-Andersen (WCA) potential to model excluded volume, and a finitely extensible nonlinear elastic (FENE) potential to mimic the covalent bonds along the strand.

We also introduce a term to add stiffness to the structure, a three-body potential (V_{semiflex}) that tends to align three consecutive beads which results in a different persistence length between single and double strands (see IIC). To model the stacking of bases in DNA/RNA, we incorporate a term called V_{stack} . This term promotes the alignment of the directions \vec{a}_1 , which determine the patch positions, of consecutive beads by using a cosine-angle potential.

For the non-bonded interactions, we used the WCA potential to account for excluded-volume interactions. Additionally, we employ a patch-patch interaction potential, based on the functional form proposed by Stillinger and Weber⁵⁵, to model the hybridization of nucleotides. The strength of the attraction between two beads i and j , ϵ_{ij} , depends on the types of nucleotides described by each interacting bead and is computed with a NN model as described below. To ensure that each bead can bind to only one other bead, we implement a repulsive three-body interaction (V_{3b}) that penalizes the formation of triplets of bonded beads⁵⁶. This repulsive potential compensates for the gain associated with the formation of a second bond and can be tuned to favor bond swapping. More, specifically, the parameter λ in V_{3b} allows to interpolate between the limits of swapping ($\lambda = 1$) and non-swapping ($\lambda \gg 1$) bonds. Finally, the V_{sticky} potential is modulated by a term V_{direct} that takes into account the \vec{a}_3 orientations of the beads to ensure that only antiparallel strands can bind to each

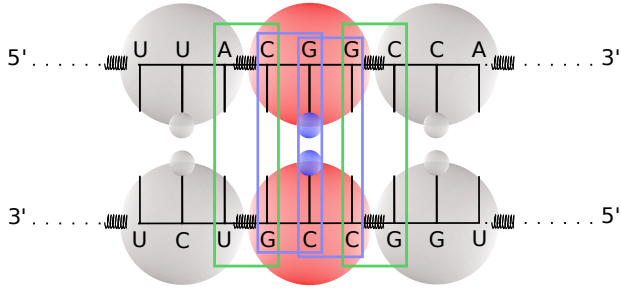


Figure 2. Contributions to the interaction strength between the two colored (red) beads, illustrating the base steps involved. The blue boxes surround base steps made of nucleotides within the beads, while the green boxes surround the two boundary base steps (*i.e.* base steps comprising nucleotides both inside and outside of the beads considered).

other.

In the following, we run molecular dynamics simulations at constant temperature⁵⁷ using the nNxB model implemented in the oxDNA simulation engine⁵⁸. The equations of motion are integrated with a velocity Verlet algorithm with a time step $\Delta t = 0.002$ (in internal units).

A. Parametrization

The strength of the sticky interaction between any two beads i, j is controlled by a term $\beta \epsilon_{ij}$ that depends on the nucleotide sequences present in each bead. This term models the pairing of the nucleotides that compose the two beads by taking into account the Gibbs free energy, multiplied by β , as provided by the nearest-neighbor model. In the following we will consider systems simulated at a fixed monovalent salt concentration of 0.5 M, but any other condition can be considered, as long as the NN model employed supports it.

In order to properly account for temperature variations, we need to separate the contributions from enthalpy and entropy. This can be achieved by rewriting $-\Delta G/k_B T$ as follows:

$$\begin{aligned} -\frac{\Delta G}{k_B T} &= -\left(\frac{\Delta H}{k_B T} - \frac{\Delta S}{k_B}\right) \\ &= -\left(\frac{\Delta H}{k_B T_{\text{ref}}} \frac{k_B T_{\text{ref}}}{k_B T} - \frac{\Delta S}{k_B}\right) \\ &= -\left(\mu \frac{\Delta H}{k_B T_{\text{ref}}} - \frac{\Delta S}{k_B}\right), \end{aligned} \quad (2)$$

where $\mu \equiv T_{\text{ref}}/T$ is a parameter that quantifies the temperature difference between the simulation temperature and the temperature T_{ref} used to estimate the values of $\Delta H, \Delta S, \Delta G$ as reported in NN models. Typically, as it is the case here, $T_{\text{ref}} = 37^\circ \text{C}$.

When calculating the ΔG between two beads, each bead should not be considered in isolation but as part of a larger system, and the coarse-graining procedure should also take into account the nucleotide base steps at the boundaries of the

beads. This means including the last nucleotide of the previous bead and the first nucleotide of the following bead for each pair of beads involved in the interaction calculation. However, in order to not overestimate the bead-bead free-energy contribution, the interactions involving nucleotides outside the considered beads are halved. As an example, consider two sequences: $5' - (..A)(CGG)(C..).....((..G)(CCG)(U..) - 3'$ (see Figure 2). The ΔH and ΔS for the interaction between the two middle beads will have the following contributions:

$$\begin{aligned} &\left(\frac{5' - A}{3' - U}\right)(CGG)(C - 3') = \\ &\frac{1}{2} \left(\frac{AC}{UG}\right) + \left(\frac{CG}{GC}\right) + \left(\frac{GG}{CC}\right) + \frac{1}{2} \left(\frac{GC}{CG}\right). \end{aligned} \quad (3)$$

In order to establish a meaningful correspondence between the potential used in our simulations and the NN parameters, the attraction strength between two beads i and j , ϵ_{ij} , is computed by equaling the free-energy change due to a bond with that predicted by the NN model, $\Delta H + T\Delta S$ ⁵⁹, which for the form and parameters of the bead-bead attraction used here yields

$$\beta \epsilon_{ij} = -\frac{1}{\alpha} \left[\left(\mu \frac{\Delta H}{k_B T_{37}} - \frac{\Delta S}{k_B} \right) + \ln(\rho^* \sigma^3 \tilde{V}_b) \right], \quad (4)$$

where $\rho^* = [\phi] \mathcal{N}_A = 6.022 \times 10^{26} \text{ m}^{-3}$ is the standard number density, σ is the diameter of the beads and corresponds to 0.79 nm (see Figure 1b), while $\tilde{V}_b = 0.0019$ and $\alpha = 0.89$ are computed via Monte Carlo integration (see Appendix B for additional details).

We note that ϵ_{ij} is the only parameter affected by the type and nature of the nucleotides: the geometry and structure of the strands are otherwise independent of the nucleic acid modeled (DNA or RNA) and bead sequence.

B. Bead design

The loss of resolution caused by dividing a strand into beads of n nucleotides leads to a problem where native motifs (e.g. hairpins in natural RNAs or crossovers in origami structures) may contain nucleotides from multiple beads or a motif may occur in the middle of a bead. We do not want, however, to make each bead correspond to a unique interaction, thereby losing the ability to simulate unintended folds caused by competing complementary sequences. To balance these competing demands, our bead design is based on the native contacts observed in folded or designed structures, with the aim of having the majority of the beads representing the same number of nucleotides, n . The optimal number of nucleotides per bead is determined by the desired level of detail and the specific system at hand, and it is set before running the simulation. However, we allow for a small fraction of the remaining beads to deviate by one nucleotide, either more or less, from the standard length, n .

As a consequence, the beads are composed of varying numbers of nucleotides, requiring the establishment of a rule for

calculating interactions. Specifically, we use the strongest ΔG found by pairing the shorter bead with all possible subsequences of the same length contained within the longer bead. In the following, we choose $n = 3$ as the standard size of the beads.

C. Parameters tuning

The free parameters of the model are the strength, denoted as k_s , and width parameter, ξ , of the V_{semiflex} potential, as well as the stacking strength, η , of the V_{stacking} potential. We optimize the values of these quantities by comparing to the melting temperatures of DNA hairpins predicted by the empirically-parameterized oxDNA model and to the persistence lengths of single- and double-stranded DNA. For the thermodynamic data, we focus on two sets of hairpins: twelve hairpins with a stem length of six and a loop length of six, and twelve hairpins with a stem length of six and a loop length of nine. The melting temperature is defined as the temperature at which the yield of the closed hairpin is 0.5, and the hairpin is considered closed when at least 3 nucleotides are bonded for oxDNA simulations), or one bead-bead bond is present, for the nNxB model. The estimation of the persistence lengths is carried out by simulating 200-beads hairpins with stems of 98 beads, and 100-beads single strands. In both cases, we define the unit vector \hat{v}_i connecting each pair i and $i + 1$, and define $\cos(\theta_{ij}) = \hat{v}_i \cdot \hat{v}_j$, where i and j are separated by m beads. Averaging over all pairs (excluding the terminal 10 beads), we obtain an angular correlation, $\langle \cos(\theta_{ij}) \rangle$, which is a function of m only. For worm-like chains, such a correlation decays as

$$\langle \cos(\theta_{ij}) \rangle = e^{-m/l_p}. \quad (5)$$

We apply Eq. (5) to extract the persistence length from our simulations. The potential we use tends to favor the presence of kinks in double strands, which decreases their persistence length. Therefore, we perform the analysis described above with and without kinks, which are defined as i, j neighboring pairs for which $\cos(\theta_{ij}) < 0.7$. While the proper persistence length requires that all angles are taken into account, excluding kinks provides an estimate of the rigidity of the double-stranded parts of the structures that do not bend much, which is the most common state of double strands in complex structures (*i.e.* origami).

In our approach, we divide the DNA sequence into groups of three nucleotides to form beads. Through extensive analysis, we found that the closest results to the oxDNA predictions and the estimated persistence length for single- and double-stranded DNA are obtained when using $\beta k_s = 4$, $\xi = 0.07$ and $\beta \eta = 6$. The resulting melting temperatures are shown in Table I, comparing very well to those extracted from oxDNA simulations. Indeed, the two data sets differ by an average of just about two kelvins.

Figure 3 illustrates that the persistence length of the double strand is approximately 28 beads with kinks and 49 without kinks, equivalent to around 84 and 147 base pairs (bp). In contrast, the derived persistence length of single strands is

approximately 3 beads, corresponding to 9 bp. These values align well with estimates for real DNA, where the persistence length of double-stranded DNA is approximately 50 nm⁶⁰ (equivalent to around 147 bp), and that of single-stranded DNA is approximately (1.98 ± 0.72) nm⁶¹ (equivalent to approximately (5.8 ± 2.1) bp), considering a base pair spacing of 0.34 nm.

Since our model accommodates representing a variable number of nucleotides per bead, to achieve a consistent persistence length in base pairs (bp), regardless of the number of nucleotides represented by the bead, it is possible to keep the parameters ξ and η constant while only adjusting the parameter k_s to achieve the desired persistence length.

6stem6loop	oxDNA	nNxB	Δ
DNAh1	66	67	1
DNAh2	72	70	-2
DNAh3	64	64	0
DNAh4	61	59	-2
DNAh5	64	67	3
DNAh6	64	62	-2
DNAh7	68	64	-4
DNAh8	71	69	-2
DNAh9	63	65	2
DNAh10	60	59	-1
DNAh11	65	64	-1
DNAh12	65	68	3
			$\langle \Delta \rangle$
			1.9

6stem9loop	oxDNA	nNxB	Δ
DNAh1	62	65	3
DNAh2	66	67	1
DNAh3	60	61	1
DNAh4	57	56	-1
DNAh5	60	64	4
DNAh6	59	60	1
DNAh7	61	62	1
DNAh8	65	66	1
DNAh9	59	62	3
DNAh10	56	56	0
DNAh11	59	62	3
DNAh12	60	65	5
			$\langle \Delta \rangle$
			2.0

Table I. Melting temperatures in °C. $|\Delta|$ is the absolute value of the difference between the oxDNA and nNxB predictions, and $\langle |\Delta| \rangle$ is its average.

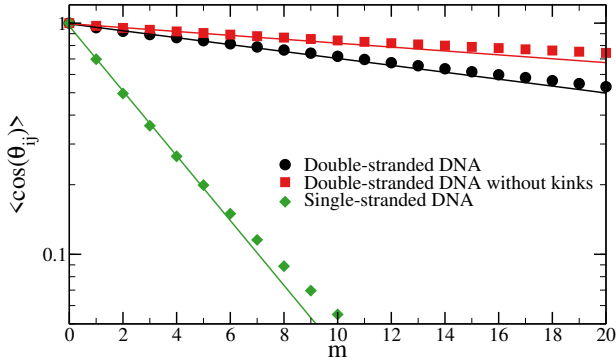


Figure 3. Angular correlation as a function of the chemical distance m for double-stranded and single-stranded DNA molecules. Points are simulation data, lines are exponential fits performed in the $m \in [0, 5]$ interval. Note that, as for real DNA and RNA, single strands do not behave as worm-like chains and therefore the angular correlation decays only approximately as an exponential.

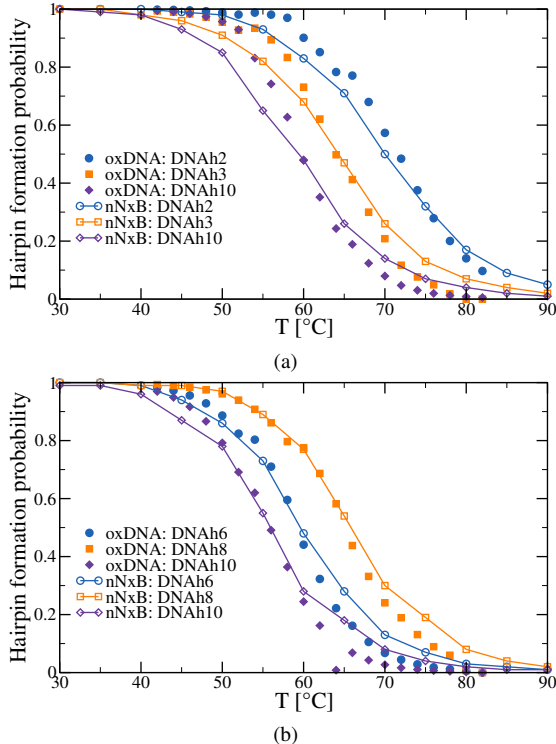


Figure 4. Comparison of the melting curves predicted by oxDNA (points) and nNxB (lines) for selected DNA hairpins with a stem length of six and a loop length of six (a), and selected DNA hairpins with a stem length of six and a loop length of nine (b). The resulting melting temperatures are listed in Table I.

III. RESULTS

A. Melting curves of hairpins

We start by comparing the melting curves of DNA hairpins simulated with oxDNA and nNxB. A hairpin is considered closed when at least half of the nucleotides in the stem, or

equivalently half of the beads, is bonded. A representative set of these results, taken from the dataset used to tune the model parameters (see Table I), is shown in Fig. 4. For all the hairpins considered, the agreement is almost quantitative for a large temperature range, with oxDNA hairpins exhibiting a somewhat narrower transition, *i.e.* slightly steeper melting curves. At high temperatures the nNxB seems to fall off more slowly compared to oxDNA: we ascribe this behavior to the fact that the bonding volume of bead-bead interactions is rather large, so that there is always a sizeable chance that two beads are considered to be bonded for purely geometrical reasons even for temperatures at which the attraction strength is small compared to the thermal energy.

We use hairpin systems to also estimate the performance difference between oxDNA and nNxB. Specifically, we run single-core molecular dynamics simulations of hairpins at the melting temperature and count the number of transitions between the two states (open and closed). Dividing the resulting number by the simulation wall time yields a factor of ≈ 100 , which we use to estimate the sampling speed-up of the new model compared to oxDNA. While the precise figure should (and will) depend on the system at hand, it is reasonable to expect the speed-up to be of the same order of magnitude, independently on the specific conditions.

B. Pseudoknot

A pseudoknot is a complex folding pattern that can occur in RNA molecules. It involves the formation of additional base pairs between distant regions of the RNA sequence, resulting in a knot-like structure. Pseudoknots are known to have crucial functions in various biological processes such as regulation of gene expression and ribosome function⁶², and viral replication⁶³. They have also been proposed to have a notable influence on RNA folding pathways⁶⁴. The thermodynamics of pseudoknot base-pairing remains poorly experimentally characterized due to their enormous diversity and complexity. Furthermore, the fact that they are composed of non-nested base pairs means that they cannot be computed using the efficient dynamic-programming approaches which dominate in the RNA secondary structure prediction field⁶⁵. Therefore, exact and heuristic coarse-graining methods have mainly focused on pseudoknot-free secondary structures.

We test our model by exploring the melting curve of the well-known MMTV pseudoknot⁶⁶. We divide the sequence in beads as depicted in Figure 5a and we compare our predictions with experimental calorimetry measurements⁶⁶ and oxRNA simulations³⁰, in Figure 5b. The yields of the two pseudoknot-precursor motifs (hairpin 1 and 2, highlighted in blue and red in Fig. 5a) display the same qualitative trends observed in oxRNA (reported in Ref.³⁰), although the peaks for hairpin 1 and hairpin 2 are higher and lower in nNxB compared to oxRNA, respectively. Summing up the yields of the two intermediate hairpins we obtain a curve (gold points in the figure) whose intersection with the single strand and pseudoknot data identifies the two transition temperatures, 83 °C and 92 °C. Compared to the experimental temperatures (74 °C and

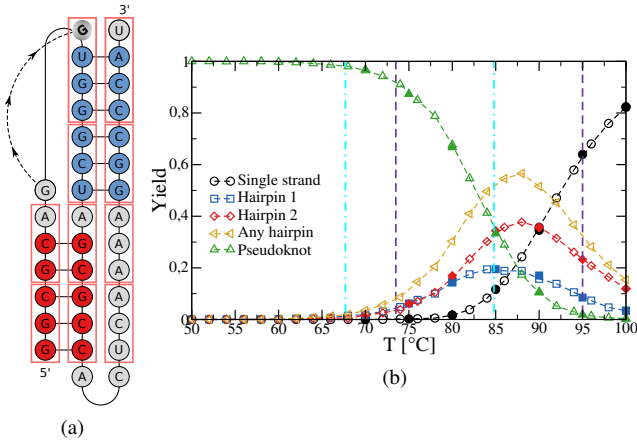


Figure 5. (a) A schematic representation of the secondary structure of the MMTV pseudoknot, showing the bead division used to simulate the strand with nNxB. Nucleotides inside the same box belong to the same bead, while nucleotides outside the box belong to the bead that follows. (b) nNxB equilibrium yields for the MMTV pseudoknot. Filled symbols represent the results of simulations without swapping, while empty symbols represent those with swapping. The transition temperatures determined experimentally⁶⁶ and numerically, with oxRNA³⁰, are indicated by violet dashed lines and cyan dash-dotted lines, respectively.

95 °C), these values are at least as good as the ones obtained with oxRNA simulations (68 °C and 85 °C) which, given the lower resolution and much higher computational efficiency of the nNxB compare to the latter, is an excellent result.

We have also run simulations without the swap mechanism, which when enabled serves the purpose of speeding up equilibration and sampling, by setting $\lambda = 10$. As shown in Figure 5b, the results obtained with and without the swap (empty and full symbols, respectively) overlap perfectly, demonstrating that the thermodynamics is not affected by the value of λ .

C. Tile

Drawing inspiration from the idea of molecular tiles, which are individual units that self-assemble to create intricate patterns or structures⁶⁷, we simulated the assembly of a single-stranded RNA tile containing a k-type pseudoknot⁶⁸.

Unfortunately, no comparison with oxRNA is possible, as observing the folding of such a structure, composed of 132 nucleotides, is currently out of reach from the computational point of view. As before, we split the sequence into beads of average size 3, but optimize the division by hand so that nucleotides that are supposed to be paired in the native structure belong to the same beads.

We simulate a single tile for different values of μ (which corresponds to different temperatures), evaluating the fraction of bonds between any two beads, and between beads that should be bonded in the native structure. The results are shown in Fig. 6 and should be compared with the dashed horizontal line that signals the fraction of bonds that are bonded

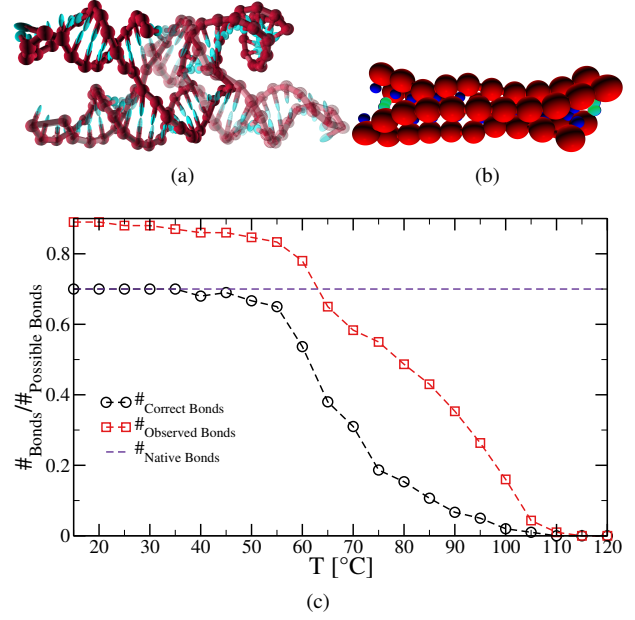


Figure 6. (a) The RNA tile composed of 132 nucleotides⁶⁸ we simulate, as represented by oxRNA. (b) A nNxB configuration simulated at 28°C. The highlighted (green) patches form kissing loops. (c) Melting curve of the RNA tile simulated with the nNxB model.

in the native structure (≈ 0.7). The nNxB model predicts a melting temperature (*i.e.* a temperature at which half of the native contacts are formed) around 65°, and that below $\approx 50^\circ$ nearly all bonds are formed.

At low temperatures, on top of the native contacts, which are always formed, we observe additional bonds that link beads that are not fully compatible with each other. Figure 7 shows the tile sequence, the splitting into beads and the native contacts (blue lines), as well as the most probable misbonds observed (red lines). It is clear that most misbonds happen between beads that are part of hairpin loops, thereby forming so-called kissing loops (highlighted in figure 6b). Kissing loops complexes are known to play an important role in RNA-RNA interactions, both in the biological and nanotechnology contexts^{69–71}. Although it is hard to estimate the stability of these motifs within the tile with oxRNA or similar coarse-grained models, the lack of flexibility of the tile arms should disfavor these particular kissing loops. Therefore, it is possible that the nNxB model overestimates their stability.

IV. DISCUSSION AND CONCLUSIONS

This study presents a novel coarse-grained model aimed at simulating folding processes of DNA and RNA nanostructures, nNxB. By representing n nucleotides with a single patchy particle, we have achieved a balance between computational efficiency and the ability to capture the interactions that govern folding dynamics, as demonstrated by simulations of DNA hairpins, an RNA pseudoknot and an RNA tile.

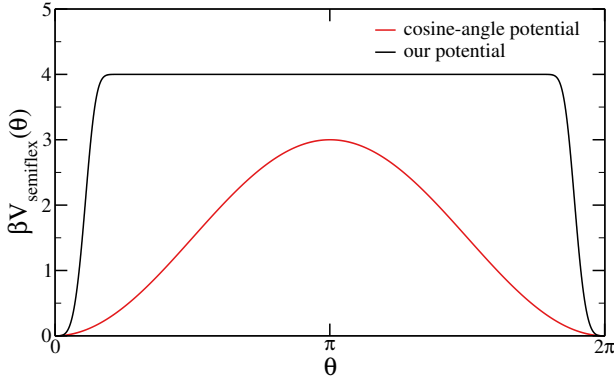


Figure 9. Plot depicting a potential designed to simulate the distinct behaviors of DNA/RNA in single- and double-stranded configurations (black curve). A widely used cosine-angle potential to introduce structural rigidity is included for comparison (red curve). The advantage of our potential is that when there are fewer constraints like in the single-stranded case, the polymer is more likely to rotate freely.

- The same WCA potential, Eq. (A1), is used to model the excluded-volume interaction;
- An attractive potential that models the hybridization of nucleotides, $V_{\text{sticky}} \cdot V_{\text{direct}}$. Each patch has a position that is given by the position of the bead it is attached to plus $\delta_{pb}\vec{a}_1$, where $\delta_{pb} = 0.65\sigma$, and $V_{\text{sticky}}(r_{pp})$ acts between any two patches. Its functional form was proposed by Stillinger and Weber⁵⁵ (see Figure 10) and reads

$$V_{\text{sticky}}^{ij}(r_{pp}) = A\epsilon_{ij} \left[B \left(\frac{\sigma_s}{r_{pp}} \right)^4 - 1 \right] e^{\sigma_s/(r_{pp}-r_c)} \quad (\text{A5})$$

where i and j are the bead types and r_{pp} is the distance between the patches and

$$\begin{aligned} B &= \frac{1}{1 + 4(1 - r_s)^2}, \\ A &= -\frac{1}{B-1} \frac{1}{e^{1/(1-r_s)}}, \\ r_c &= \sigma_s r_s. \end{aligned} \quad (\text{A6})$$

The coefficient ϵ_{ij} modulates the strength of the sticky attraction and depends on what nucleotides are inside the considered beads (see Section II A). We set $\epsilon_{ij} \neq 0$ only if the chemical distance between i and j is larger than two, since a loop of just 6 nucleotides does not occur in DNA/RNA strands. This potential depends essentially on two parameters: σ_s , which defines the minimum of the potential (*i.e.* the radius of the patch) and is set to 0.21875σ , and r_s , which defines the steepness of the potential between the minimum and r_c (set to 0.35), after which $V_{\text{sticky}} = 0$. Thus, two particles are bonded if the relative distance between their patches is less than r_c . The directionality of DNA/RNA is enforced by multiplying V_{sticky} by a term acting on the \vec{a}_3 directions of

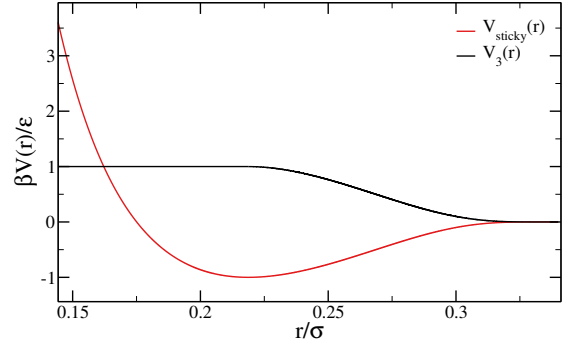


Figure 10. The different potentials acting between non-bonded beads.

beads:

$$V_{\text{direct}}(\vec{a}_3^{(i)}, \vec{a}_3^{(j)}) = \frac{\vec{a}_3^{(i)} \cdot \vec{a}_3^{(j)}}{2}. \quad (\text{A7})$$

This term makes sure that only antiparallel strands can bind to each other.

- V_{3b} , To ensure that each bead interacts only with one other, we implement a repulsive three-body interaction V_{3b} which penalizes the formation of triplets of bonded beads⁵⁶. In particular, V_{3b} is designed to almost exactly compensate the gain associated with the formation of a second bond, originating an almost flat energy hypersurface that favors bond swapping even in the presence of pair attraction energies much larger than the thermal energy. This repulsive potential is defined as

$$V_{3b} = \lambda \sum_{ijk} \min(\epsilon_{ij}, \epsilon_{ik}) V_3(r_{ij}) V_3(r_{ik}) \quad (\text{A8})$$

where the sum runs over all triplets of bonded particles (bead i bonded both with k and j), whereas we took the minimum between ϵ_{ij} and ϵ_{ik} to favor the removal of the more loosely bonded bead. r_{ij} is the distance between bead i and j . The value of the parameter λ allows to interpolate between the limits of swapping ($\lambda = 1$) and non-swapping ($\lambda \gg 1$) bonds. The pair potential $V_3(r)$ is defined in terms of the normalized $V_{\text{sticky}}(r)$ as

$$V_3(r) = \begin{cases} 1, & r \leq \sigma_s \\ -\frac{V_{\text{sticky}}^{ij}(r)}{\epsilon_{ij}}, & \sigma_s \leq r \leq r_c \end{cases} \quad (\text{A9})$$

where σ_s is the distance at which $V_{\text{sticky}}^{ij}(r)$ has a minimum.

Appendix B: Mapping

To find a suitable mapping between the potential used in our simulations and experimental data we followed the procedure of Ref.⁵⁹: we consider the hybridization of two single-stranded portions A and B to give a hybridized (double-stranded) molecule AB:

$$A + B \rightleftharpoons AB \quad (\text{B1})$$

for which the equilibrium constant can be written as

$$K = \frac{[AB]/[\ominus]}{([A]/[\ominus])([B]/[\ominus])} = \frac{\rho_{AB}\rho^\ominus}{\rho_A\rho_B} = \exp(-\beta\Delta G^\ominus), \quad (\text{B2})$$

where $[\ominus] = 1 \text{ mol dm}^{-3}$ is the standard state concentration, $\rho^\ominus = [\ominus]\mathcal{N}_A = 6.022 \times 10^{26} \text{ m}^{-3}$ is the standard number density and ΔG^\ominus is the standard Gibbs energy for the transformation given in eq.B1 where 50% of the monomers have hybridized. In our model, this hybridization free energy is obtained from a nearest-neighbor thermodynamic model. Assuming that the solution of monomers and dimers is ideal, which is reasonable provided the concentration of each species is small, we can write the canonical partition function of each species x (where x can be A, B, or AB) as:

$$Q_x = \frac{V^{N_x}}{N_x!\Lambda_x^{3N_x}} q_x^{N_x} \quad (\text{B3})$$

where V is the volume of the container, N_x is the number of particles of species x , Λ_x is the de Broglie thermal wavelength of species x and q_x is the internal partition function of species x . Each of the chemical potentials can straightforwardly be calculated from the canonical partition function:

$$\mu_x = -k_B T \frac{\partial \ln Q_x}{\partial N_x} = k_B T \ln(\rho_x \Lambda_x^3 / q_x). \quad (\text{B4})$$

At the equilibrium, $\mu_A + \mu_B = \mu_{AB}$, which we can solve as:

$$\frac{\rho_{AB}}{\rho_A\rho_B} = \frac{q_{AB}\Lambda_A^3\Lambda_B^3}{q_Aq_B\Lambda_{AB}^3} \quad (\text{B5})$$

We assume that the internal state of the monomeric units that bind is not affected by binding. We express this by setting the internal partition functions of the two monomers equal to unity, $q_A = q_B = 1$. Moreover, since the AB molecule is described classically as a dimer of the A and B particles, the de Broglie thermal wavelengths cancel out, since the momenta of the two monomeric units in the dimer are uncoupled, The rotational partition function of the dimer is thus subsumed into the translational degrees of freedom of the constituting monomers, given that we integrate over the potential energy over all possible states; we include this contribution in the internal partition function q_{AB} , which will therefore have dimensions of volume. Hence, we have:

$$\frac{\rho_{AB}}{\rho_A\rho_B} = q_{AB}. \quad (\text{B6})$$

and by comparing this equation with eq.B2 we can write:

$$q_{AB}\rho^\ominus = \exp(-\beta\Delta G^\ominus). \quad (\text{B7})$$

Knowing that:

$$q_{AB} = 4\pi \int r^2 dr \int d\{\vec{a}\} \int d\{\vec{b}\} e^{-\beta V} \quad (\text{B8})$$

where V is the total interaction potential between the two beads.

We evaluate the right-hand side of Eq. B8 by means of a Monte Carlo integration, finding that, for $\epsilon \gtrsim 3$, $q_{AB} \simeq V_b e^{\alpha\beta\epsilon}$, where $V_b = 0.0019 \sigma^3$ and $\alpha = 0.89$ are fitting parameters. Substituting this relation in eq.B7 we find

$$\tilde{V}_b e^{\alpha\beta\epsilon_{ij}} \sigma^3 \rho^\ominus = e^{-\beta\Delta G^\ominus}, \quad (\text{B9})$$

so that

$$\begin{aligned} \ln(\rho^\ominus \sigma^3 \tilde{V}_b) + \alpha\beta\epsilon_{ij} &= -\beta\Delta G^\ominus \\ \beta\epsilon_{ij} &= -\frac{1}{\alpha} [\beta\Delta G^\ominus + \ln(\rho^\ominus \sigma^3 \tilde{V}_b)] \end{aligned} \quad (\text{B10})$$

Since $\Delta G = \Delta H - T\Delta S$, we can rewrite the previous equation as:

$$\beta\epsilon_{ij} = -\frac{1}{\alpha} \left[\frac{1}{k_B T} (\Delta H - T\Delta S) + \ln(\rho^\ominus \sigma^3 \tilde{V}_b) \right], \quad (\text{B11})$$

Using eq.2, we obtain:

$$\beta\epsilon_{ij} = -\frac{1}{\alpha} \left[\left(\mu \frac{\Delta H}{k_B T_{37}} - \frac{\Delta S}{k_B} \right) + \ln(\rho^\ominus \sigma^3 \tilde{V}_b) \right]. \quad (\text{B12})$$

REFERENCES

- ¹S. Pitchiaya and Y. Krishnan, “First blueprint, now bricks: Dna as construction material on the nanoscale,” *Chemical Society Reviews* **35**, 1111–1121 (2006).
- ²S. Dey, C. Fan, K. V. Gothelf, J. Li, C. Lin, L. Liu, N. Liu, M. A. Nijenhuis, B. Saccà, F. C. Simmel, *et al.*, “Dna origami,” *Nature Reviews Methods Primers* **1**, 13 (2021).
- ³I. Tinoco Jr and C. Bustamante, “How rna folds,” *Journal of molecular biology* **293**, 271–281 (1999).
- ⁴Z. Tang, X. Zhang, Y. Shu, M. Guo, H. Zhang, and W. Tao, “Insights from nanotechnology in covid-19 treatment,” *Nano today* **36**, 101019 (2021).
- ⁵S. Li, Q. Jiang, S. Liu, Y. Zhang, Y. Tian, C. Song, J. Wang, Y. Zou, G. J. Anderson, J.-Y. Han, *et al.*, “A dna nanorobot functions as a cancer therapeutic in response to a molecular trigger in vivo,” *Nature biotechnology* **36**, 258–264 (2018).
- ⁶Y. Benenson, “Rna-based computation in live cells,” *Current opinion in biotechnology* **20**, 471–478 (2009).
- ⁷C. Du, P. Hu, and L. Ren, “Nucleic acid-based scaffold systems and application in enzyme cascade catalysis,” *Applied Microbiology and Biotechnology* **107**, 9–23 (2023).
- ⁸N. C. Seeman, “Nanomaterials based on dna,” *Annual review of biochemistry* **79**, 65–87 (2010).
- ⁹P. W. Rothmund, “Folding dna to create nanoscale shapes and patterns,” *Nature* **440**, 297–302 (2006).
- ¹⁰S. M. Douglas, H. Dietz, T. Liedl, B. Högberg, F. Graf, and W. M. Shih, “Self-assembly of dna into nanoscale three-dimensional shapes,” *Nature* **459**, 414–418 (2009).
- ¹¹J. Bath, S. J. Green, K. E. Allen, and A. J. Turberfield, “Mechanism for a directional, processive, and reversible dna motor,” *Small* **5**, 1513–1516 (2009).
- ¹²T. E. Ouldridge, R. L. Hoare, A. A. Louis, J. P. Doye, J. Bath, and A. J. Turberfield, “Optimizing dna nanotechnology through coarse-grained modeling: a two-footed dna walker,” *ACS nano* **7**, 2479–2490 (2013).
- ¹³X. Shi, A.-K. Pumm, C. Maffeo, F. Kohler, E. Feigl, W. Zhao, D. Verschuere, R. Golestanian, A. Aksimentiev, H. Dietz, *et al.*, “A dna turbine powered by a transmembrane potential across a nanopore,” *Nature Nanotechnology*, 1–7 (2023).

- ¹⁴L. M. Adleman, "Molecular computation of solutions to combinatorial problems," *science* **266**, 1021–1024 (1994).
- ¹⁵Y.-J. Chen, N. Dalchau, N. Srinivas, A. Phillips, L. Cardelli, D. Soloveichik, and G. Seelig, "Programmable chemical controllers made from dna," *Nature nanotechnology* **8**, 755–762 (2013).
- ¹⁶B. Wang, S. S. Wang, C. Chalk, A. D. Ellington, and D. Soloveichik, "Parallel molecular computation on digital data stored in dna," *Proceedings of the National Academy of Sciences* **120**, e2217330120 (2023).
- ¹⁷W. D. Cornell, P. Cieplak, C. I. Bayly, I. R. Gould, K. M. Merz, D. M. Ferguson, D. C. Spellmeyer, T. Fox, J. W. Caldwell, and P. A. Kollman, "A second generation force field for the simulation of proteins, nucleic acids, and organic molecules," *Journal of the American Chemical Society* **117**, 5179–5197 (1995).
- ¹⁸B. R. Brooks, R. E. Bruccoleri, B. D. Olafson, D. J. States, S. a. Swaminathan, and M. Karplus, "Charmm: a program for macromolecular energy, minimization, and dynamics calculations," *Journal of computational chemistry* **4**, 187–217 (1983).
- ¹⁹J. Spöner, G. Bussi, M. Krepl, P. Banáš, S. Bottaro, R. A. Cunha, A. Gil-Ley, G. Pinamonti, S. Poblete, P. Jurecka, *et al.*, "Rna structural dynamics as captured by molecular simulations: a comprehensive overview," *Chemical reviews* **118**, 4177–4338 (2018).
- ²⁰M. Parisien and F. Major, "The mc-fold and mc-sym pipeline infers rna structure from sequence data," *Nature* **452**, 51–55 (2008).
- ²¹A. Savelyev and G. A. Papoian, "Molecular renormalization group coarse-graining of polymer chains: application to double-stranded dna," *Biophysical Journal* **96**, 4044–4052 (2009).
- ²²M. Paliy, R. Melnik, and B. A. Shapiro, "Coarse-graining rna nanostructures for molecular dynamics simulations," *Physical biology* **7**, 036001 (2010).
- ²³S. Pasquali and P. Derreumaux, "Hire-rna: a high resolution coarse-grained energy model for rna," *The journal of physical chemistry B* **114**, 11957–11966 (2010).
- ²⁴T. E. Ouldridge, A. A. Louis, and J. P. Doye, "Structural, mechanical, and thermodynamic properties of a coarse-grained dna model," *The Journal of chemical physics* **134**, 02B627 (2011).
- ²⁵P. Šulc, F. Romano, T. E. Ouldridge, L. Rovigatti, J. P. Doye, and A. A. Louis, "Sequence-dependent thermodynamics of a coarse-grained dna model," *The Journal of chemical physics* **137**, 135101 (2012).
- ²⁶D. M. Hinckley, G. S. Freeman, J. K. Whitmer, and J. J. De Pablo, "An experimentally-informed coarse-grained 3-site-per-nucleotide model of dna: Structure, thermodynamics, and dynamics of hybridization," *The Journal of chemical physics* **139**, 10B604_1 (2013).
- ²⁷T. Cragolini, P. Derreumaux, and S. Pasquali, "Coarse-grained simulations of rna and dna duplexes," *The Journal of Physical Chemistry B* **117**, 8047–8060 (2013).
- ²⁸Z. Xia, D. R. Bell, Y. Shi, and P. Ren, "Rna 3d structure prediction by using a coarse-grained model and experimental data," *The Journal of Physical Chemistry B* **117**, 3135–3144 (2013).
- ²⁹N. A. Denesyuk and D. Thirumalai, "Coarse-grained model for predicting rna folding thermodynamics," *The Journal of Physical Chemistry B* **117**, 4901–4911 (2013).
- ³⁰P. Šulc, F. Romano, T. E. Ouldridge, J. P. Doye, and A. A. Louis, "A nucleotide-level coarse-grained model of rna," *The Journal of chemical physics* **140**, 06B614_1 (2014).
- ³¹N. Korolev, D. Luo, A. P. Lyubartsev, and L. Nordenskiöld, "A coarse-grained dna model parameterized from atomistic simulations by inverse monte carlo," *Polymers* **6**, 1655–1675 (2014).
- ³²M. Maciejczyk, A. Spasic, A. Liwo, and H. A. Scheraga, "Dna duplex formation with a coarse-grained model," *Journal of chemical theory and computation* **10**, 5020–5035 (2014).
- ³³C. Maffeo, T. T. Ngo, T. Ha, and A. Aksimentiev, "A coarse-grained model of unstructured single-stranded dna derived from atomistic simulation and single-molecule experiment," *Journal of chemical theory and computation* **10**, 2891–2896 (2014).
- ³⁴L. Rovigatti, P. Šulc, I. Z. Reguly, and F. Romano, "A comparison between parallelization approaches in molecular dynamics simulations on gpu," *Journal of computational chemistry* **36**, 1–8 (2015).
- ³⁵M. R. Machado and S. Pantano, "Exploring laci–dna dynamics by multi-scale simulations using the sirah force field," *Journal of chemical theory and computation* **11**, 5012–5023 (2015).
- ³⁶J. J. Uusitalo, H. I. Ingoólfsson, P. Akhshi, D. P. Tieleman, and S. J. Marrink, "Martini coarse-grained force field: extension to dna," *Journal of chemical theory and computation* **11**, 3932–3945 (2015).
- ³⁷P. D. Dans, J. Walther, H. Gómez, and M. Orozco, "Multiscale simulation of dna," *Current opinion in structural biology* **37**, 29–45 (2016).
- ³⁸I. Ivani, P. D. Dans, A. Noy, A. Pérez, I. Faustino, A. Hospital, J. Walther, P. Andrio, R. Gofñi, A. Balaceanu, *et al.*, "Parmbsc1: a refined force field for dna simulations," *Nature methods* **13**, 55–58 (2016).
- ³⁹D. Chakraborty, N. Hori, and D. Thirumalai, "Sequence-dependent three interaction site model for single- and double-stranded dna," *Journal of chemical theory and computation* **14**, 3763–3779 (2018).
- ⁴⁰C. Maffeo and A. Aksimentiev, "Mrdna: a multi-resolution model for predicting the structure and dynamics of dna systems," *Nucleic acids research* **48**, 5135–5146 (2020).
- ⁴¹M. DeLuca, T. Ye, M. Poirier, Y. Ke, C. Castro, and G. Arya, "Mechanism of dna origami folding elucidated by mesoscopic simulations," *bioRxiv* (2023), 10.1101/2023.06.20.545758.
- ⁴²A. Sengar, T. E. Ouldridge, O. Henrich, L. Rovigatti, and P. Šulc, "A primer on the oxdna model of dna: when to use it, how to simulate it and how to interpret the results," *Frontiers in Molecular Biosciences* **8**, 693710 (2021).
- ⁴³D. Poland and H. A. Scheraga, "Occurrence of a phase transition in nucleic acid models," *The Journal of chemical physics* **45**, 1464–1469 (1966).
- ⁴⁴J. SantaLucia Jr and D. Hicks, "The thermodynamics of dna structural motifs," *Annu. Rev. Biophys. Biomol. Struct.* **33**, 415–440 (2004).
- ⁴⁵H. T. Allawi and J. SantaLucia, "Nearest-neighbor thermodynamics of internal a-c mismatches in dna: Sequence dependence and ph effects," *Biochemistry* **37**, 9435–9444 (1998).
- ⁴⁶H. T. Allawi and J. SantaLucia Jr, "Thermodynamics of internal c-t mismatches in dna," *Nucleic acids research* **26**, 2694–2701 (1998).
- ⁴⁷H. T. Allawi and J. SantaLucia, "Nearest neighbor thermodynamic parameters for internal g-c mismatches in dna," *Biochemistry* **37**, 2170–2179 (1998).
- ⁴⁸H. T. Allawi and J. SantaLucia, "Thermodynamics and nmr of internal g-c t mismatches in dna," *Biochemistry* **36**, 10581–10594 (1997).
- ⁴⁹N. Peyret, P. A. Seneviratne, H. T. Allawi, and J. SantaLucia, "Nearest-neighbor thermodynamics and nmr of dna sequences with internal a-c, c-g, g-c, and t-c t mismatches," *Biochemistry* **38**, 3468–3477 (1999).
- ⁵⁰D. H. Turner and D. H. Mathews, "Nndb: the nearest neighbor parameter database for predicting stability of nucleic acid secondary structure," *Nucleic acids research* **38**, D280–D282 (2010).
- ⁵¹J. M. Huguette, C. V. Bizarro, N. Forns, S. B. Smith, C. Bustamante, and F. Ritort, "Single-molecule derivation of salt dependent base-pair free energies in dna," *Proceedings of the National Academy of Sciences* **107**, 15431–15436 (2010).
- ⁵²J. H. Bae, J. Z. Fang, and D. Y. Zhang, "High-throughput methods for measuring dna thermodynamics," *Nucleic acids research* **48**, e89–e89 (2020).
- ⁵³J. Zuber, S. J. Schroeder, H. Sun, D. H. Turner, and D. H. Mathews, "Nearest neighbor rules for rna helix folding thermodynamics: improved end effects," *Nucleic Acids Research* **50**, 5251–5262 (2022).
- ⁵⁴G. S. Grest and K. Kremer, "Molecular dynamics simulation for polymers in the presence of a heat bath," *Physical Review A* **33**, 3628 (1986).
- ⁵⁵T. A. Weber and F. H. Stillinger, "Local order and structural transitions in amorphous metal-metalloid alloys," *Physical Review B* **31**, 1954 (1985).
- ⁵⁶F. Sciortino, "Three-body potential for simulating bond swaps in molecular dynamics," *The European Physical Journal E* **40**, 1–4 (2017).
- ⁵⁷J. Russo, P. Tartaglia, and F. Sciortino, "Reversible gels of patchy particles: role of the valence," *The Journal of Chemical Physics* **131**, 014504 (2009).
- ⁵⁸E. Poppleton, M. Matthies, D. Mandal, F. Romano, P. Šulc, and L. Rovigatti, "oxdna: coarse-grained simulations of nucleic acids made simple," *Journal of Open Source Software* **8**, 4693 (2023).
- ⁵⁹A. Reinhardt and D. Frenkel, "Dna brick self-assembly with an off-lattice potential," *Soft Matter* **12**, 6253–6260 (2016).
- ⁶⁰M. D. Wang, H. Yin, R. Landick, J. Gelles, and S. M. Block, "Stretching dna with optical tweezers," *Biophysical journal* **72**, 1335–1346 (1997).
- ⁶¹E. Roth, A. Glick Azaria, O. Girshevitz, A. Bitler, and Y. Garini, "Measuring the conformation and persistence length of single-stranded dna using a dna origami structure," *Nano letters* **18**, 6703–6709 (2018).
- ⁶²A. Peselis and A. Serganov, "Structure and function of pseudoknots involved in gene expression control," *Wiley Interdisciplinary Reviews: RNA* **5**, 803–822 (2014).

- ⁶³K. Neupane, M. Zhao, A. Lyons, S. Munshi, S. M. Ileperuma, D. B. Ritchie, N. Q. Hoffer, A. Narayan, and M. T. Woodside, "Structural dynamics of single sars-cov-2 pseudoknot molecules reveal topologically distinct conformers," *Nature Communications* **12**, 4749 (2021).
- ⁶⁴M. Kucharik, I. L. Hofacker, P. F. Stadler, and J. Qin, "Pseudoknots in rna folding landscapes," *Bioinformatics* **32**, 187–194 (2016).
- ⁶⁵S. R. Eddy, "How do rna folding algorithms work?" *Nature biotechnology* **22**, 1457–1458 (2004).
- ⁶⁶C. A. THEIMER and D. P. GIEDROC, "Contribution of the intercalated adenosine at the helical junction to the stability of the gag-pro frameshifting pseudoknot from mouse mammary tumor virus," *RNA* **6**, 409–421 (2000).
- ⁶⁷E. Winfree, F. Liu, L. A. Wenzler, and N. C. Seeman, "Design and self-assembly of two-dimensional dna crystals," *Nature* **394**, 539–544 (1998).
- ⁶⁸E. Poppleton, J. Bohlin, M. Matthies, S. Sharma, F. Zhang, and P. Šulc, "Design, optimization and analysis of large dna and rna nanostructures through interactive visualization, editing and molecular simulation," *Nucleic acids research* **48**, e72–e72 (2020).
- ⁶⁹J.-C. Paillart, E. Skripkin, B. Ehresmann, C. Ehresmann, and R. Marquet, "A loop-loop" kissing" complex is the essential part of the dimer linkage of genomic hiv-1 rna." *Proceedings of the National Academy of Sciences* **93**, 5572–5577 (1996).
- ⁷⁰E. Bindewald, R. Hayes, Y. G. Yingling, W. Kasprzak, and B. A. Shapiro, "Rnajunction: a database of rna junctions and kissing loops for three-dimensional structural analysis and nanodesign," *Nucleic acids research* **36**, D392–D397 (2008).
- ⁷¹D. Liu, C. W. Geary, G. Chen, Y. Shao, M. Li, C. Mao, E. S. Andersen, J. A. Piccirilli, P. W. Rothmund, and Y. Weizmann, "Branched kissing loops for the construction of diverse rna homooligomeric nanostructures," *Nature Chemistry* **12**, 249–259 (2020).
- ⁷²D. Han, X. Qi, C. Myhrvold, B. Wang, M. Dai, S. Jiang, M. Bates, Y. Liu, B. An, F. Zhang, *et al.*, "Single-stranded dna and rna origami," *Science* **358**, eaao2648 (2017).
- ⁷³X. Qi, F. Zhang, Z. Su, S. Jiang, D. Han, B. Ding, Y. Liu, W. Chiu, P. Yin, and H. Yan, "Programming molecular topologies from single-stranded nucleic acids," *Nature communications* **9**, 4579 (2018).
- ⁷⁴K. Leppek, G. W. Byeon, W. Kladwang, H. K. Wayment-Steele, C. H. Kerr, A. F. Xu, D. S. Kim, V. V. Topkar, C. Choe, D. Rothschild, *et al.*, "Combinatorial optimization of mrna structure, stability, and translation for rna-based therapeutics," *Nature communications* **13**, 1536 (2022).
- ⁷⁵Y.-A. Kim, K. Mousavi, A. Yazdi, M. Zwierzyna, M. Cardinali, D. Fox, T. Peel, J. Collier, K. Aggarwal, and G. Maruggi, "Computational design of mrna vaccines," *Vaccine* (2023), <https://doi.org/10.1016/j.vaccine.2023.07.024>.
- ⁷⁶A. L. Božič, C. Micheletti, R. Podgornik, and L. Tubiana, "Compactness of viral genomes: effect of disperse and localized random mutations," *Journal of Physics: Condensed Matter* **30**, 084006 (2018).
- ⁷⁷D. Vauptič, A. Rosa, L. Tubiana, and A. Božič, "Scaling properties of RNA as a randomly branching polymer," *The Journal of Chemical Physics* **158**, 234901 (2023).
- ⁷⁸S. Gambietz, L. J. Stenke, and B. Saccà, "Sequence-dependent folding of monolayered dna origami domains," *Nanoscale* **15**, 13120–13132 (2023).
- ⁷⁹A. Cumberworth, D. Frenkel, and A. Reinhardt, "Simulations of dna-origami self-assembly reveal design-dependent nucleation barriers," *Nano Letters* **22**, 6916–6922 (2022), pMID: 36037484.
- ⁸⁰R. Veneziano, S. Ratanalert, K. Zhang, F. Zhang, H. Yan, W. Chiu, and M. Bathe, "Designer nanoscale dna assemblies programmed from the top down," *Science* **352**, 1534–1534 (2016).
- ⁸¹D. H. Mathews, M. D. Disney, J. L. Childs, S. J. Schroeder, M. Zuker, and D. H. Turner, "Incorporating chemical modification constraints into a dynamic programming algorithm for prediction of rna secondary structure," *Proceedings of the National Academy of Sciences* **101**, 7287–7292 (2004).
- ⁸²J. P. Doye, T. E. Ouldridge, A. A. Louis, F. Romano, P. Šulc, C. Matek, B. E. Snodin, L. Rovigatti, J. S. Schreck, R. M. Harrison, *et al.*, "Coarse-graining dna for simulations of dna nanotechnology," *Physical Chemistry Chemical Physics* **15**, 20395–20414 (2013).
- ⁸³C. Hyeon, R. I. Dima, and D. Thirumalai, "Size, shape, and flexibility of rna structures," *The Journal of chemical physics* **125**, 194905 (2006).
- ⁸⁴J. Abels, F. Moreno-Herrero, T. Van der Heijden, C. Dekker, and N. H. Dekker, "Single-molecule measurements of the persistence length of double-stranded rna," *Biophysical journal* **88**, 2737–2744 (2005).
- ⁸⁵G. M. Studnicka, G. M. Rahn, I. W. Cummings, and W. A. Salser, "Computer method for predicting the secondary structure of single-stranded rna," *Nucleic Acids Research* **5**, 3365–3388 (1978).
- ⁸⁶M. Antczak, M. Popena, T. Zok, M. Zurkowski, R. W. Adamiak, and M. Szachniuk, "New algorithms to represent complex pseudoknotted rna structures in dot-bracket notation," *Bioinformatics* **34**, 1304–1312 (2018).
- ⁸⁷M. Bon, G. Vernizzi, H. Orland, and A. Zee, "Topological classification of rna structures," *Journal of molecular biology* **379**, 900–911 (2008).
- ⁸⁸L. M. Hochrein, M. Schwarzkopf, M. Shahgholi, P. Yin, and N. A. Pierce, "Conditional dicer substrate formation via shape and sequence transduction with small conditional rnas," *Journal of the American Chemical Society* **135**, 17322–17330 (2013).
- ⁸⁹T. E. Ouldridge, P. Šulc, F. Romano, J. P. Doye, and A. A. Louis, "Dna hybridization kinetics: zippering, internal displacement and sequence dependence," *Nucleic acids research* **41**, 8886–8895 (2013).
- ⁹⁰N. Srinivas, T. E. Ouldridge, P. Šulc, J. M. Schaeffer, B. Yurke, A. A. Louis, J. P. Doye, and E. Winfree, "On the biophysics and kinetics of toehold-mediated dna strand displacement," *Nucleic acids research* **41**, 10641–10658 (2013).
- ⁹¹P. Imisch, T. E. Ouldridge, and R. Seidel, "Modeling dna-strand displacement reactions in the presence of base-pair mismatches," *Journal of the American Chemical Society* **142**, 11451–11463 (2020).
- ⁹²F. Romano, D. Chakraborty, J. P. Doye, T. E. Ouldridge, and A. A. Louis, "Coarse-grained simulations of dna overstretching," *The Journal of chemical physics* **138**, 02B610 (2013).
- ⁹³Q. Wang and B. M. Pettitt, "Modeling dna thermodynamics under torsional stress," *Biophysical journal* **106**, 1182–1193 (2014).
- ⁹⁴T. Sutthibutpong, C. Matek, C. Benham, G. G. Slade, A. Noy, C. Laughton, J. P. K. Doye, A. A. Louis, and S. A. Harris, "Long-range correlations in the mechanics of small dna circles under topological stress revealed by multi-scale simulation," *Nucleic acids research* **44**, 9121–9130 (2016).
- ⁹⁵L. Rovigatti, F. Bomboi, and F. Sciortino, "Accurate phase diagram of tetravalent dna nanostars," *The Journal of Chemical Physics* **140**, 154903 (2014).
- ⁹⁶M. C. Engel, F. Romano, A. A. Louis, and J. P. Doye, "Measuring internal forces in single-stranded dna: Application to a dna force clamp," *Journal of chemical theory and computation* **16**, 7764–7775 (2020).